JOURNAL OF GEOPHYSICAL RESEARCH, VOL. 88, NO. A5, PAGES 4027–4040, MAY 1, 1983

Sounder-Accelerated Particles Observed on ISIS

H. G. JAMES

Communications Research Centre, Department of Communications, Ottawa, Ontario, Canada K2H 8S7

The soft-particle spectrometers aboard the spacecrafts ISIS I and ISIS II detect sounder-accelerated particles, i.e., fluxes of electrons and ions energized by the 100-μs transmitter pulse (nominal peak power: 400 W). Fluxes of up to 10^8 st^{-1} eV^{-1} cm^{-2} s^{-1} are observed. Typical highest electron and ion energies are several hundred electronvolts and 100–200 eV, respectively. Sounder-accelerated electron fluxes detected on ISIS II are energized near the major electron resonant frequencies: f_{pe} (plasma frequency), f_{ce} (gyrofrequency), $2f_{ce}$ and the oblique resonance frequency domains. Ion fluxes are present from the lowest sounder frequency (0.1 MHz) up to the greater of f_{pe} and f_{ce}. Electrons are observed at pitch angles near 90° while ions are present at all pitch angles. The observations can be interpreted using a model of particle motion and spacecraft dc potential both induced by the intense rf field (~100 V/m). The ion results indicate that at $f < f_{pe}, f_{ce}$, a negative potential of about 100 V is on the spacecraft, whereas at $f > f_{pe}, f_{ce}$, the potential is much smaller. ISIS I data from equatorial perigee conditions show that electrons remain energized for a few milliseconds after the end of the rf pulse.

INTRODUCTION

The use of high-frequency transmitters in the ionosphere, notably the topside sounder spacecraft, has led to the discovery of a diversity of plasma wave effects. The most successful analyses of electromagnetic (EM) and electrostatic (ES) waves have been based on linear geometric-optics properties of radiated waves (*Muldrew* [1972] and references therein). A number of authors have dealt with the comparatively difficult topics of nonlinear phenomena close to the spacecraft (*Hagg et al.* [1969], *Benson* [1982], and references therein). Theoretical analyses of nonlinearities have mostly been based on concepts of interacting waves.

The domain of antenna-plasma nonlinearities, say in the first few meters around the active antenna, has received little attention. Yet, processes occurring in this region are surely at the origin of many nonlinear phenomena observed by the topside sounders.

The investigation of sounder-accelerated particles (SAP) can provide a much improved picture of this little known domain. Research in this general area goes back at least to the investigation of the behavior of rf antennas on rocket bodies (*Whale* [1964] and references therein). Early work considered the ponderomotive force on electrons [*Getmantsev and Denisov*, 1962] as an essential ingredient for the sheath description. Later work refined the calculation of the impedance of various probes including the dipole antenna, for frequencies well below the electron resonant frequencies [*Shkarofsky*, 1972] and well above (*Laframboise et al.* [1975] and references therein).

The work of *Oya* [1971, 1978] and *Benson* [1982] is representative of a class of research which considers energization near an ionospheric antenna brought about by electrostatic (ES) wave absorption. Although the physical scale in question much exceeds that of the SAP model to be discussed, there may be some common ground in the explanations of SAP and of wave-absorption heating.

Until very recently, experimental antenna research has been mostly limited to antenna driving-point or radiation-field quantities [*Balmain*, 1979]. The work of *Gal'perin et al.* [1981] is one of the first to present independent particle measurements in the near environment of an active antenna. They report on the existence of 100-eV electrons energized by 133-μs pulses from the sounder transmitter on the Interkosmos 19 (IK 19) spacecraft. IK 19 used an electrostatic spectrometer to detect SAP in the energy range 10 eV to 500 eV, on rare occasions at 1 keV. Operating in the 500–1000 km altitude range, IK 19 typically received strong SAP when the sounder frequency was at 0.7–0.8 of the plasma frequency. The SAP fluxes lasted up to 3 ms after the end of the rf pulses, and were strongest at night.

The relative strength of SAP at equatorial latitudes led Gal'perin and co-workers to discuss geophysically favorable conditions for particle acceleration. They propose that SAP effects can accumulate from successive rf pulses. They also suggest radio wave trapping in low-latitude ionization ducts may be enhanced by virtue of SAP heating of the plasma in those ducts.

The present work confirms some of the observations of Gal'perin and co-workers. In several ways it complements their results by virtue of ISIS spacecraft having different orbital parameters and different transmitter and particle-detection characteristics. This investigation focusses more specifically on the spacecraft, antennas and the immediate surrounding plasma. A major concern of this article is to document the detailed dependence of SAP flux on sounder frequency, pitch angle and energy. Descriptions of the instrument and of the general observations are followed by detailed examples of SAP flux distributions, parametrical in plasma parameters, for both electrons and ions. A picture of spacecraft rf-induced potential is then compared with the evidence. Certain observations are identified which support the model.

Finally, there is a discussion of ISIS I data which show that SAP electrons remain energized for milliseconds. This section includes an analysis of electron bounce times.

The existence of SAP means that antenna plasma nonlinearities are important near the electron plasma and gyrofrequencies, respectively, f_{pe} and f_{ce}. Theories of HF antenna energetics will not be complete until they account for the SAP energization mechanism. The ISIS I results, similar to IK 19 results, indicate that the phenomenon may be used in several ways to study electrodynamics in space.

Copyright 1983 by the American Geophysical Union.

Paper number 3A0265.
0148-0227/83/003A-0265$05.00

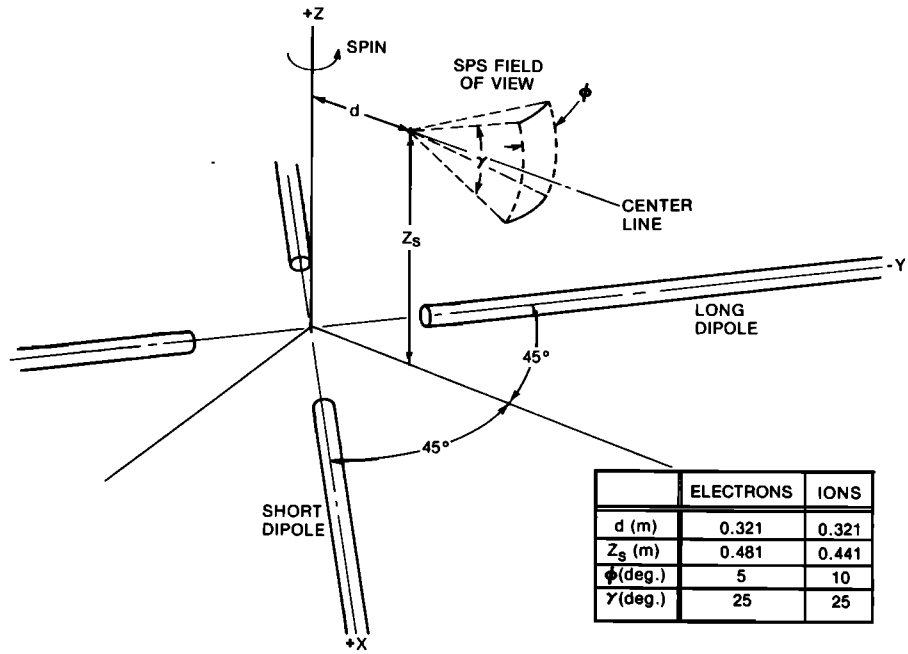

	ELECTRONS	IONS
d (m)	0.321	0.321
Z_S (m)	0.481	0.441
φ(deg.)	5	10
γ(deg.)	25	25

Fig. 1. Geometry of sounder dipoles and SPS field of view relative to ISIS II spacecraft $X-Y-Z$ axes.

INSTRUMENTS

The soft particle spectrometer (SPS) on ISIS II measures the flux of electrons and positive ions as a function of energy. The instrument actually has two spectrometers which measure electron and ion fluxes in an energy-sweep mode. The 'top beam' measures electrons while the 'bottom beam' measures ions. The two are mounted looking in identical directions perpendicular to the spacecraft spin axis (Z axis) and at a longitudinal angle of 45° with respect to the long sounder dipole (73 m tip to tip), as shown in Figure 1. The top detector has a geometric factor of 4.95×10^{-4} cm^2 st and an energy bandpass ($\Delta E/E$) of 24.7%. It has 38 effective channels at central energies logarithmically spaced between 13.15 keV and 5.5 eV. The bottom detector has a geometric factor of 1.27×10^{-3} cm^2 st and an energy bandpass ($\Delta E/E$) of 35.5% with 39 channels between 14.68 keV and 5.0 eV. Essentially the same instrument was flown on ISIS I; it is described by *Heikkila et al.* [1970].

The ISIS II sounder [*Franklin and Maclean*, 1969] emits 86-μs pulses at a pulse repetition frequency (PRF) of 45 s^{-1}. These pulses may be transmitted in a conventional ionogram format during which the carrier frequency is swept from 0.1 to 10 or 0.1 to 20 MHz in a piecewise linear-with-time fashion. Alternatively, the carrier frequency may be fixed at any one of six preset values. In both cases, the ionogram frames last about 20 s.

A cross-over network between the sounder transmitter and the sounder dipoles ensures that the long dipole is the working antenna for frequencies up to about 5 MHz, i.e., for frequencies that excite SAP. The peak rf voltage appearing at the antenna driving point is a complicated function of the frequency and plasma parameters. It undoubtedly reaches values of 1 kV at frequencies which energize SAP, as shown, for instance, in Figure 5 of *James* [1980].

The SPS repeats an energy sweep every second. As shown in Figure 2, each energy channel in the energy downsweep is sampled for 1/90 sec and this is followed by an 1/180 s

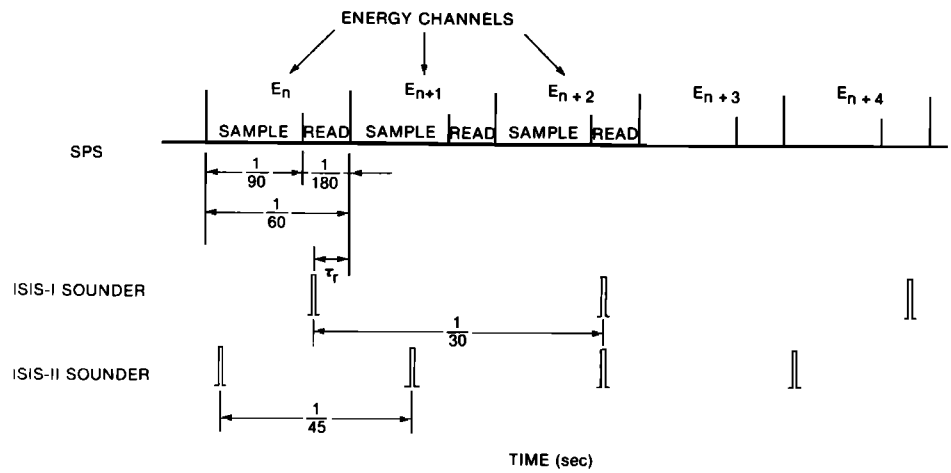

Fig. 2. Timing of SPS sample and read periods, and sounder transmit pulses. E_n labels energy of a channel. The pulse widths for ISIS I and ISIS II are 98 and 86 μs, respectively. τ_r = 4.69 ms.

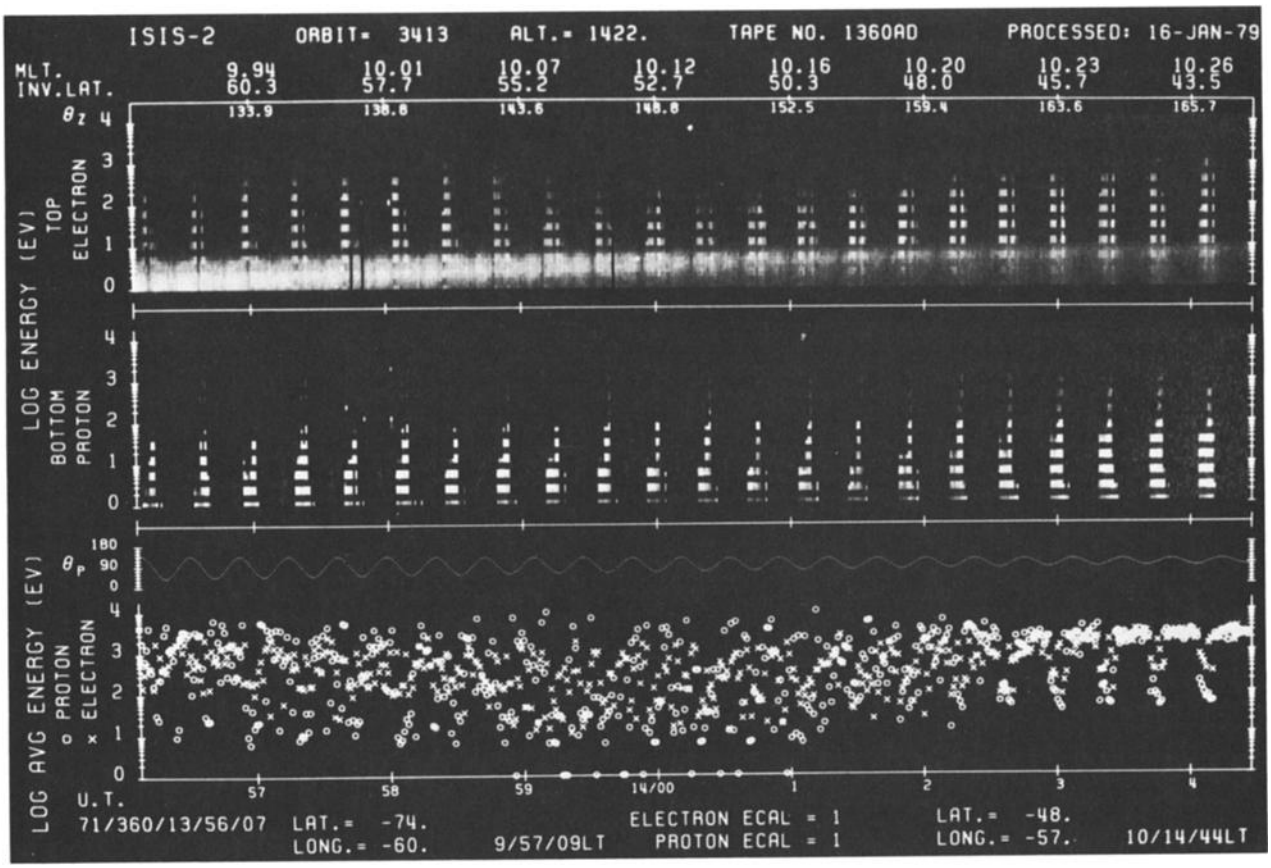

Fig. 3. SPS spectrogram showing SAP electrons as barred spikes in the upper display and SAP ions in middle display.

interval in which the accumulated counts are read out to telemetry. The timing is such as to place consecutive pulses in consecutive SPS count periods n and $n + 1$, the following pulse in readout period $n + 2$, and no pulse in period $n + 3$. The cycle then repeats. The result is the two-in, two-out pattern in the energy sweep that is observed in many SPS spectrograms from sounder-on passes of ISIS II. The pattern is shown in Figure 3.

The ISIS I satellite carries essentially the same SPS as ISIS II. However, the PRF of the ISIS I sounder is 30 s^{-1}, and the timing was purposefully designed to place the pulses in the readout interval for each SPS energy channel. Therefore, SAP is not normally expected on ISIS I. The few examples of SAP that have been identified in ISIS I spectrograms will be discussed later.

ISIS II OBSERVATIONS

General Characteristics

ISIS II has a circular orbit at about 1400 km altitude with an inclination of 88.7° prograde. SAP is observed at all latitudes, and can be found, to a greater or lesser extent, in most SPS spectrograms. Figure 3 is a spectrogram with both electron and ion data gathered during a midlatitude pass. SAP is much in evidence as the series of barred spikes at 20-s intervals. The horizontal bars attest to the aforementioned phase relation of the sounder pulses and the SPS sweep, leading to an on-off pattern in groups of two energy channels.

SAP is observed at energies from 5 eV up to about 1 keV in Figure 3. Typically electrons are limited to a few hundred electronvolts and ions to about 100 eV. In a small fraction of passes, electron energies ~1 keV and ion energies of several hundred electronvolts have been observed. In Figure 3, the combined effect of the finite SAP energy bandwidth and the two-on/two-off phasing is that SAP can be measured in about 12 energy channels of the SPS on a given pass.

Upon comparing sounder and SPS data in cases like that of Figure 3 it is found that the individual spikes each correspond to the beginning of a sounder frequency sweep. In the case of the electron data, the vertical dropout in each spike corresponds to time when the sounder frequency is in the range 0.1–0.5 MHz. For instance, such a dropout occurs at 1403:00 UT in Figure 3. SAP electrons are detected just before this when the sounder is on a 3-s fixed frequency operation at 1.00 MHz, and just after when the frequency is in the range approximately 0.5 to 2.0 MHz. Careful comparison of Figure 3 electron and ion data reveals that the longest part of the ion spikes are aligned with the vertical drop-out bars in the electron spikes. This systematic dependence of the fluxes on sounder frequency will be more fully illustrated in section 2 below. Characteristics of the energy spectrum of the fluxes are described in section 3.

A practical consequence for SPS spectrograms is that when the sounder frequency is fixed at one of the lower preset frequencies corresponding to SAP energization, the spikes are replaced by wide SAP patterns that stretch across the spectrogram and that thus tend to obliterate other (natural) fluxes that may be of interest. SAP flux intensities typically reach 10^8 cm^{-2} st^{-1} s^{-1} eV^{-1}. This of the same order as typical auroral-zone natural levels.

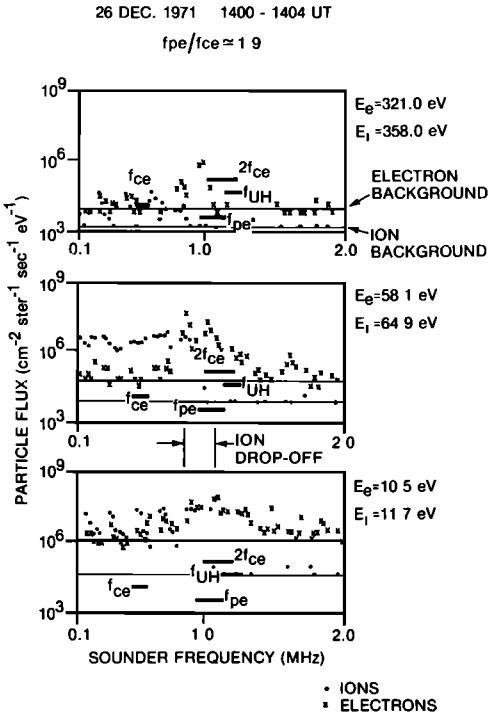

Fig. 4. SAP flux versus sounder frequency at representative energies. The short thick horizontal bars labeled f_{pe}, f_{ce}, f_{uH}, $2f_{ce}$ show the plasma parameter ranges determined from the ionograms. The thin horizontal lines give the electron (upper) and ion (lower) background fluxes. At interval midpoint, lat. = −56°, long. = −57°.

SAP Flux Versus Sounder Frequency

The data base for the study of sounder frequency dependence is 13 ISIS II passes recorded in 1971 and 1972, at a variety of latitudes. In order to reduce the variation in the important parameter pitch angle, data were selected from

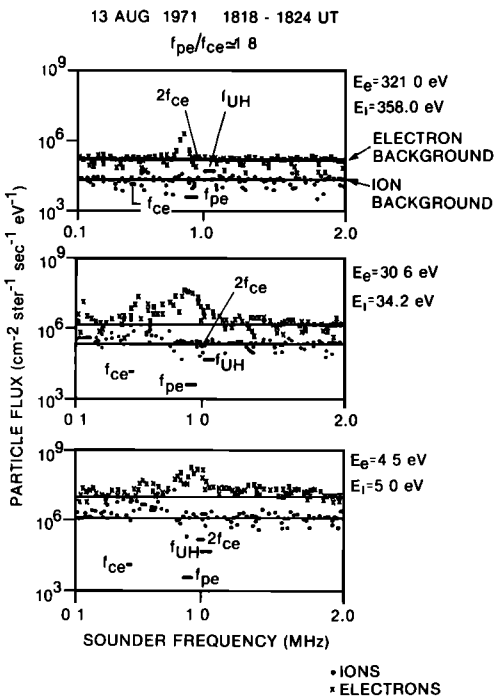

Fig. 5. See caption to Figure 4. At interval midpoint, lat. = −14°, long. = 35°.

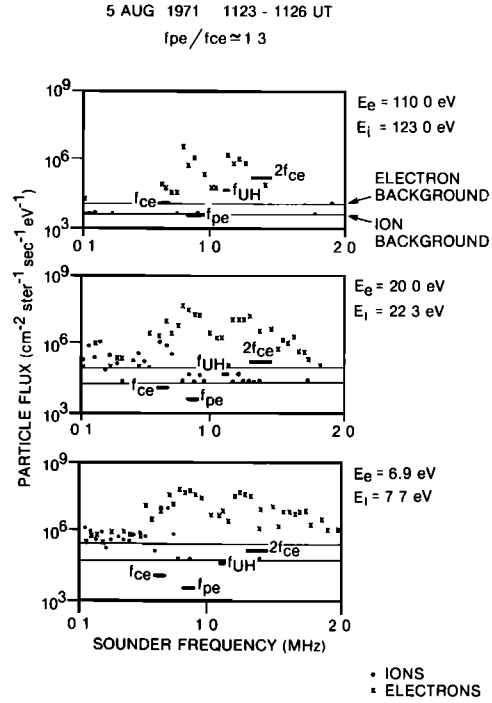

Fig. 6. See caption to Figure 4. At interval midpoint, lat. = −17°, long. = 148°.

passes during which the spacecraft spin axis was close to the orbit plane ('orbit-aligned'). In these cases the pitch angle oscillated about 90° through a range that was no larger than about 60° to 120°.

SAP fluxes exhibit strong dependence on plasma parameters, of which the ISIS II orbit provided some variety. In the data surveyed the plasma frequency f_{pe} varied in the range 0.45–1.15 MHz, and the gyrofrequency f_{ce} lay between 0.49

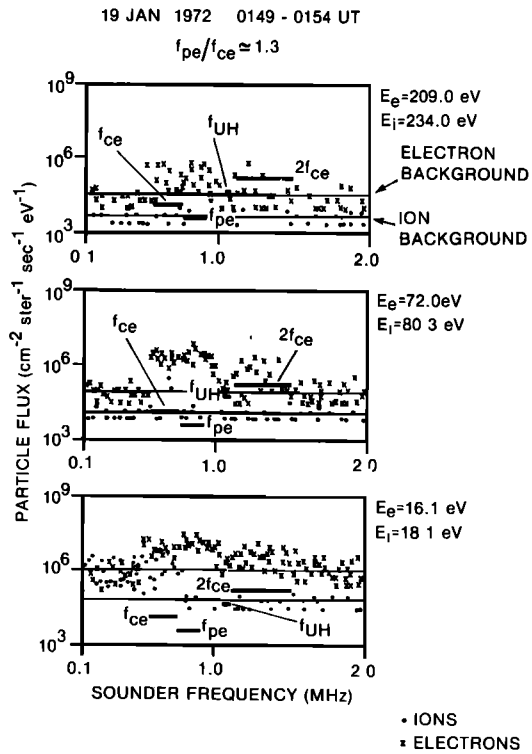

Fig. 7. See caption to Figure 4. At interval midpoint, lat. = 19°, long. = −80°.

and 0.97 MHz. In the following we discuss representative pass data intervals in which f_{pe} and f_{ce} were confined to specific ranges.

As the ratio f_{pe}/f_{ce} goes from greater than 1 to less than 1, the shape of the SAP flux versus sounder frequency changes in a systematic way. This is illustrated in the Figures 4–10. In this format, the differential electron and ion fluxes in selected representative energy channels are plotted as a function of the sounder sweep frequency in the range where the most intense SAP is observed, namely, 0.1–2.0 MHz. The data sets are taken typically from 4- to 6-min periods of ISIS II passes during which the f_{pe} and f_{ce} values, scaled from the corresponding ionograms, have remained within reasonably small bounds. These bounds are indicated by the heavy bars parallel to the frequency axis in the diagrams. The heavy bar labeled f_{UH} gives the range of the upper hybrid resonance frequency, $f_{UH} = (f_{pe}^2 + f_{ce}^2)^{1/2}$. The thin lines give the background fluxes as determined from neighboring energy channels which do not sample SAP, on account of the on/off phasing mentioned above. The ion background is always the lower line.

Case for $f_{pe} > f_{ce}$: Fluxes from three ISIS II passes in 1971 are plotted in Figures 4 to 6. Figures 4 and 5 have the highest value of f_{pe}/f_{ce}. The 321.0-eV distributions are similar to those in the work of *Gal'perin et al.* [1981], exhibiting a main peak at or near f_{pe}. The f_{pe}/f_{ce} value was higher by a factor of 2 in the data reported by Gal'perin and co-workers. A somewhat weaker peak occurs near f_{ce}. When, as in Figure 6, $2f_{ce}$ is significantly greater than f_{pe}, a separate strong maximum is seen near $2f_{ce}$.

Occasionally, other secondary peaks, more than 1 order of magnitude smaller than the main peak, appear at other frequencies. The data suggest that at the highest observed energies, i.e., at a few hundred electronvolts, the 'f_{pe} peak' is at a frequency just below the value of f_{pe} scaled from the ionogram, and that it aligns more nearly with f_{pe} as energy is decreased.

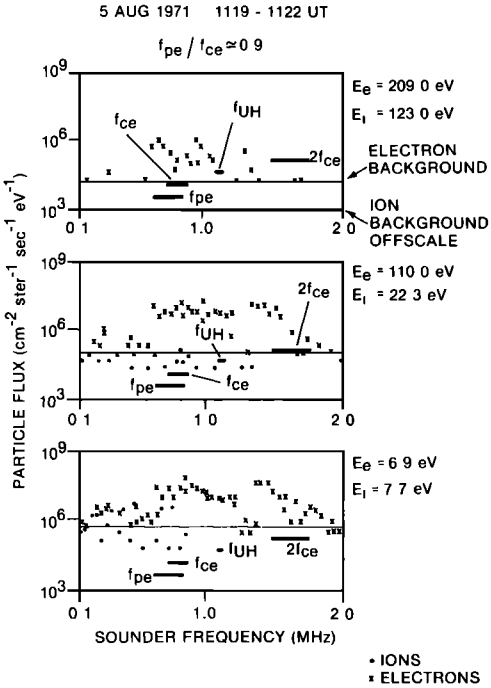

Fig. 8. See caption to Figure 4. At interval midpoint, lat. = −29°, long. = 149°.

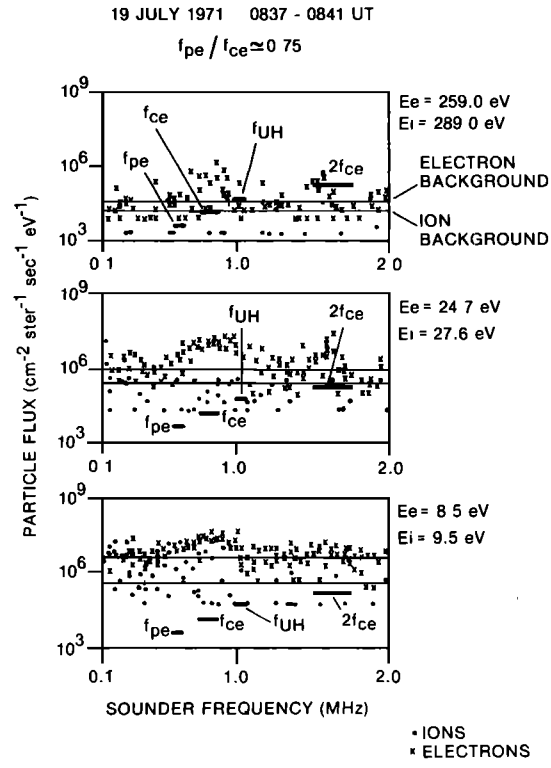

Fig. 9. See caption to Figure 4. At interval midpoint, lat. = 52°, long. = −148°.

Energetic ions are observed at energies as high as about 50 eV where they may exhibit a weak peak near f_{ce}. At lower energies, the ion fluxes fill the frequency range from 0.1 MHz up to an intermediate frequency between f_{ce} and f_{pe};

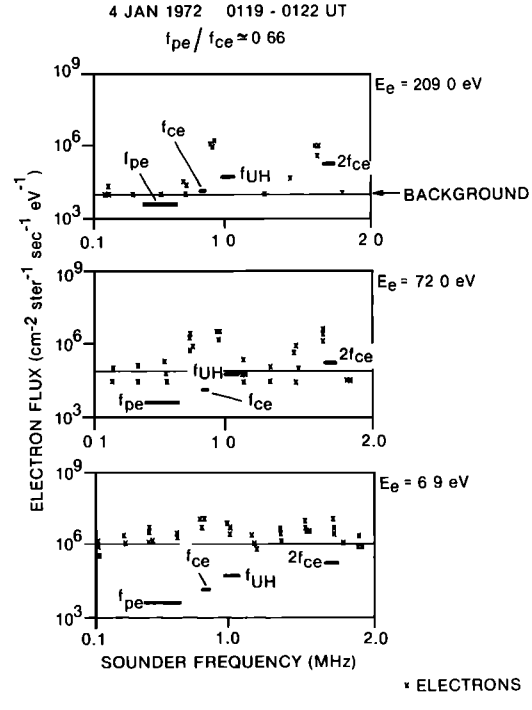

Fig. 10. SAP electron flux versus sounder frequency at representative energies. The short thick horizontal bars labeled f_{pe}, f_{ce}, f_{uh}, $2f_{ce}$ show the plasma parameter ranges determined from the ionograms. The thin horizontal line gives the background flux. At interval midpoint, lat. = 56°, long. = 129°.

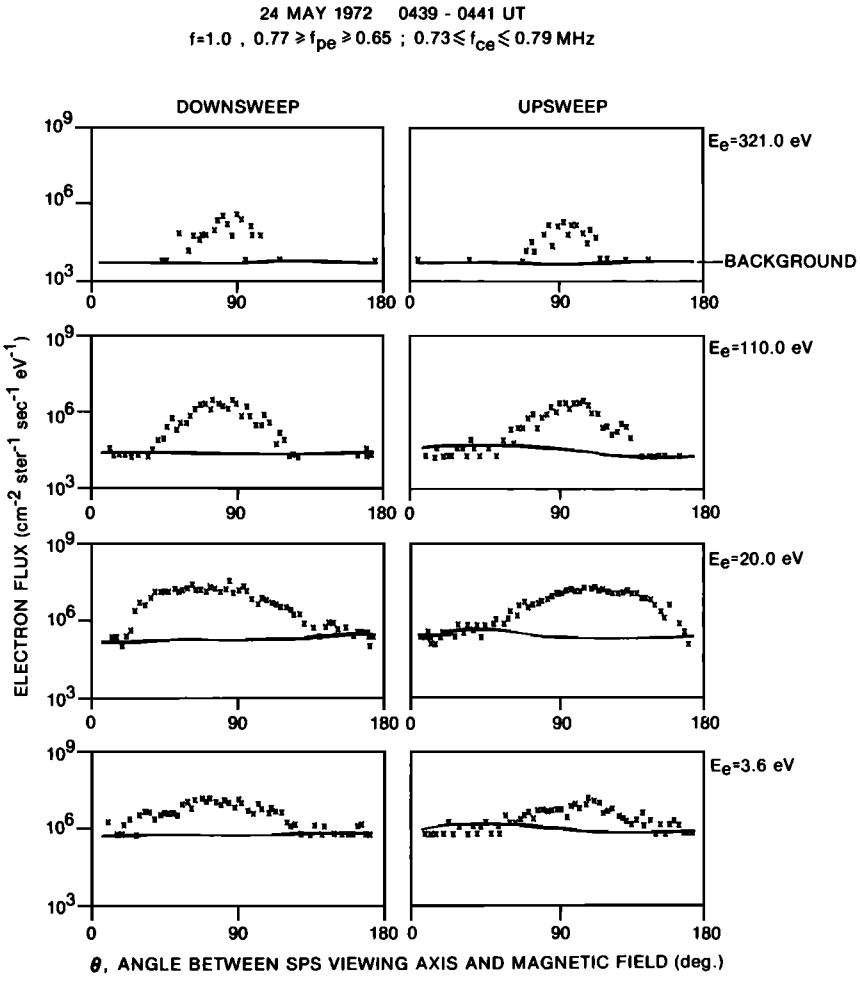

Fig. 11. SAP electron flux versus viewing angle at four typical energies for a fixed transmitter frequency of 1.0 MHz. In the 'downsweep' panel, angle θ sweeps from high to low values. The thin line gives the background flux. At interval midpoint, lat. = 31°, long. = −85°.

however, the distribution still has a broad maximum near f_{ce}.

The observed ion fluxes in the December 26 case have an unusually high upper energy limit. Also, the upper frequency limit of their distribution is atypically sharp and close to f_{pe}. A dropoff in ion fluxes as frequency sweeps through the neighborhood of f_{pe} is observed consistently in most of the data. The dropoff is labeled in Figure 4.

Case for $f_{pe} \lesssim f_{ce}$: Figures 7–10 illustrate how the flux versus frequency distributions change as f_{pe}/f_{ce} goes from about 1.2 to 0.6. As f_{ce} rises above f_{pe}, $2f_{ce}$ goes to frequencies well above f_{pe}. With this, the electron flux at frequencies around 1.5 MHz is enhanced. For instance, see the $2f_{ce}$-associated electron peaks in the middle panels of both Figures 9 and 10. This second peak level is within an order of magnitude of the main peak at high energies and of about equal intensity at lower energies. As in Figures 4–6, the overall width of the electron distribution increases with decreasing frequency.

Important electron flux peaks are still located near the f_{pe} to f_{ce} interval. However, a repeatable alignment of peaks and the f_{pe} and f_{ce} bars is not found. Sometimes, as in all panels of Figure 7, the alignment with f_{pe}, f_{ce}, and $2f_{ce}$ is good. Other times, as in the upper panel of Figure 8, the alignment is poor. Often, as in the middle panels of Figures 8, 9, and 10, there is a broad maximum that carries from f_{pe} up to f_{UH}.

SAP ions are not present in the highest energy channel of any of Figures 7–10. As energy decreases, they are first observed near f_{ce}; see the middle panels of Figures 7 and 8. Around 5–10 eV, SAP ions fill the frequency range between 0.1 and the greater of f_{pe} and f_{ce}.

Summary: At energies of about 200 eV, a narrow peak is observed near the greater of f_{pe} and f_{ce} in the SAP electron flux. At lower energies the distribution broadens and peaks appear near f_{pe}, f_{ce}, f_{UH}, and $2f_{ce}$, but do not consistently line up with any of them. SAP ions are first observed near f_{ce} as energy is reduced past about 100 eV. Ions are consistently confined to frequencies below the greater of f_{pe} and f_{ce}.

SAP Flux Versus Pitch Angle

A significant quantity of SAP data has been recorded by the SPS when the sounder was in its 'mixed' mode of operation. The mixed mode (fixed transmitter frequency, swept receiver frequency) is appropriate for study of the SAP angular distributions because the fixed transmission frequency allows the spacecraft spin effects to be isolated as a function of time. The sounder ionograms obtained during mixed mode operations provide information on the ionogram

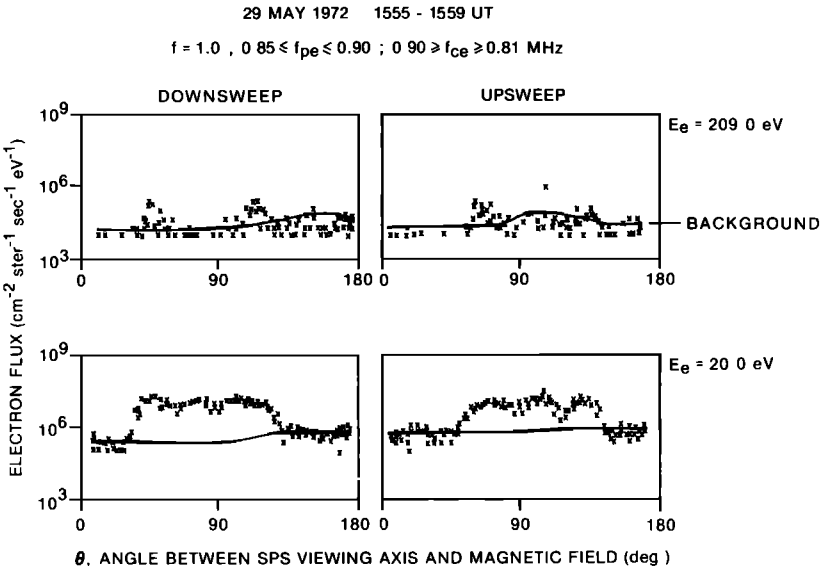

Fig. 12. SAP electron flux versus viewing angle at two typical energies for a fixed transmitter frequency of 1.0 MHz. In the 'downsweep' panel, angle θ sweeps from high to low values. The thin line gives the background flux. At interval midpoint, lat. = 43°, long. = −83°.

density, since the spectral side bands are transmitted through a wide enough frequency range to excite the principal resonance spikes, including f_{pe} [*Lockwood*, 1973].

The data discussed here come mostly from passes during which the frequency was fixed at 1.00 MHz. It will be seen from Figures 4–10 that this preset fixed frequency value fortuitously is close to the frequency of the main peaks in the flux versus frequency distributions.

Electrons: Data from eight ISIS II passes with a large sweep in pitch angle have been analyzed. These include four passes in which the antennas rotated in the orbital plane ('cartwheel' spin orientation), which is approximately the magnetic meridian plane except near the poles, and four noncartwheel passes during which spin axis was briefly at right angles to the local magnetic field. There are no essential differences between the pitch angle distributions from the two sets.

The limitation of the f_{pe} and f_{ce} values along the ISIS II orbit and the restriction of our data set to the fixed frequency of 1.00 MHz mean that the ISIS pitch angle data relate to specific areas in plasma-parameter space. For Figure 11, the transmitting frequency is near f_{UH}, given the f_{pe} and f_{ce} at the time. This situation is similar to the conditions in Figure 8, and corresponds to a point on the right shoulder of the main SAP-electron peak between f_{pe} and f_{UH} in Figure 8. The pitch angle distributions at selected energies are plotted, using an abscissa the angle θ between the magnetic field and the axis of the SPS field of view. The corresponding particle pitch angle = $\alpha = \theta + 180°$. The diagrams are split into two parts, the left part for θ going from maximum to minimum, and the right part for the θ sweep in the opposite sense.

The θ distribution has a comparatively narrow peak, about 20° to 30° wide at the 10 dB point, at the highest energies. The width varies inversely with the energy. At the highest energy, the peaks are closest to 90°, although measurably displaced from 90°. As energy decreases, the peaks shift farther away from 90° and become less symmetrical with respect to 90°.

The other parametrical situation studied is represented by the data in Figure 12, wherein f_{pe} and f_{ce} are both closer to 1.00 MHz than in Figure 11. The transmitting frequency is therefore significantly less than f_{UH} and closer to f_{ce}, f_{pe}. With reference to Figure 8, the operating point may be thought of as near, or perhaps on the left side of, the main peak. In this situation, the electron distribution at the highest energies is double-peaked and centered about a point displaced from 90° by a few degrees. As energy decreases below 100 eV, the distribution begins to fill in near $\theta = 90°$. The distribution retains this shape for all lower energies, with some second-order asymmetry.

The electron distributions in Figure 11 illustrate what is also observed on IK 19 [*Gal'perin et al.*, 1981]: SAP electrons correspond to acceleration roughly perpendicular to the magnetic field. The ISIS data, moreover, demonstrate that this occurs at all latitudes, since distributions like those in Figure 11 (geomagnetic latitude range: 39°–54°) have been obtained between 4° and 68° geomagnetic latitude. For instance, the peak electron fluxes in Figure 4 are about 10^8 at a latitude of −62°, the most poleward case plotted. By comparison, the equatorial (lat ≃ 9°) fluxes at a comparable energy in Figure 12 attain values of about 10^7.

Cyclotron pumping conventionally will energize perpendicular motion more than parallel motion. However, the observational absence of SAP electrons with $\theta \simeq 0°$, 180° does not prove that the rf field produces no energization nearly parallel to the magnetic field. A consequence of the shape of the near rf-field lines is that the field 'blows' particles away from the antenna. Computed electron trajectories show that guiding centres have a component of motion antiparallel to the local gradient in the rf field [*Johnston*, 1960]. The lack of SAP at $\theta \simeq 0°$, 180° may be conditioned by the fact that such trajectories have no access to the SPS entrance aperture. Such particles move away from the spacecraft. Therefore spacecraft like IK 19 or ISIS with collocated transmitters and particle detectors cannot strictly prove the absence of SAP with $\theta \simeq 0°$, 180°. This will have to wait until the near environment of the antenna can be explored with an independently positioned particle detector.

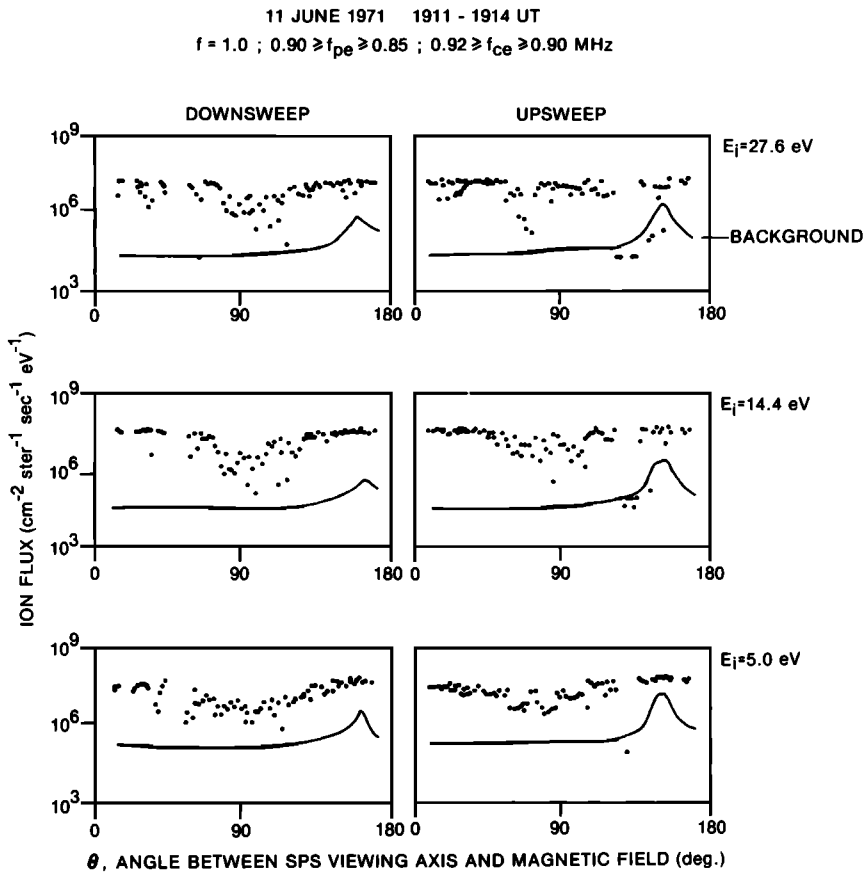

Fig. 13. SAP ion flux versus viewing angle at three typical energies for a fixed transmitter frequency of 1.0 MHz. In the 'downsweep' panel, angle θ sweeps from high to low values. The thin line gives the background flux. At interval midpoint, lat. = 57°, long. = −89°.

Future particle orbit calculations may also help to determine if SAP exists at $\theta = 0°$.

Ions: Figures 13 and 14 give examples of the flux versus θ distributions of SAP ions. The θ dependence is very slight. In these figures, the angle β between the SPS viewing axis and the satellite velocity oscillates about 90° by 20° to 30°. Other data with larger sweeps show sharp dips in flux versus β once per spin period, especially at energies below 10 eV. Those data imply that the ram effect is important for the lower energies. Also, the flux versus β plots are asymetrical.

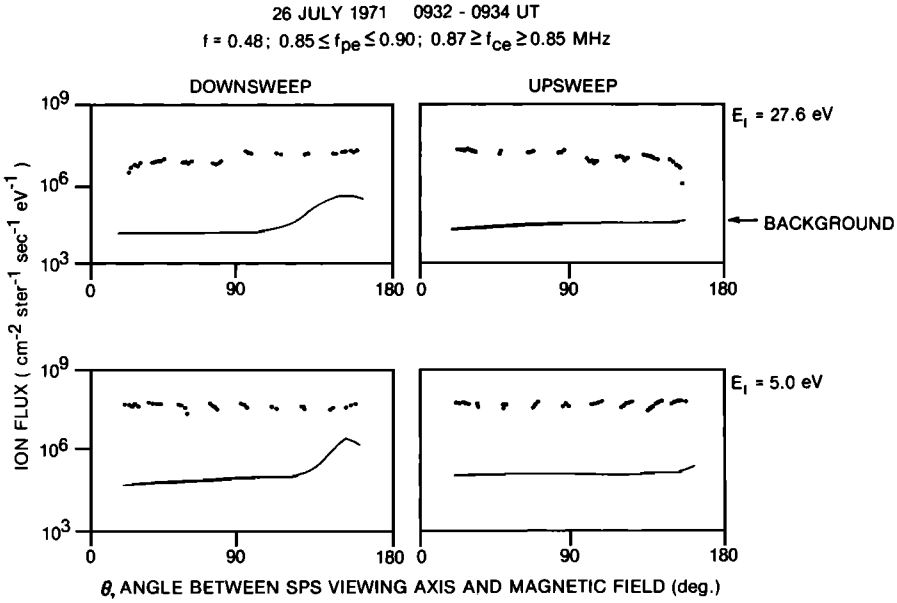

Fig. 14. SAP ion flux versus pitch angle at two typical energies for a fixed transmitter frequency of 0.48 MHz. In the 'downsweep' panel, angle θ sweeps from high to low values. The thin line gives the background flux. At interval midpoint, lat. = 74°, long. = 2°.

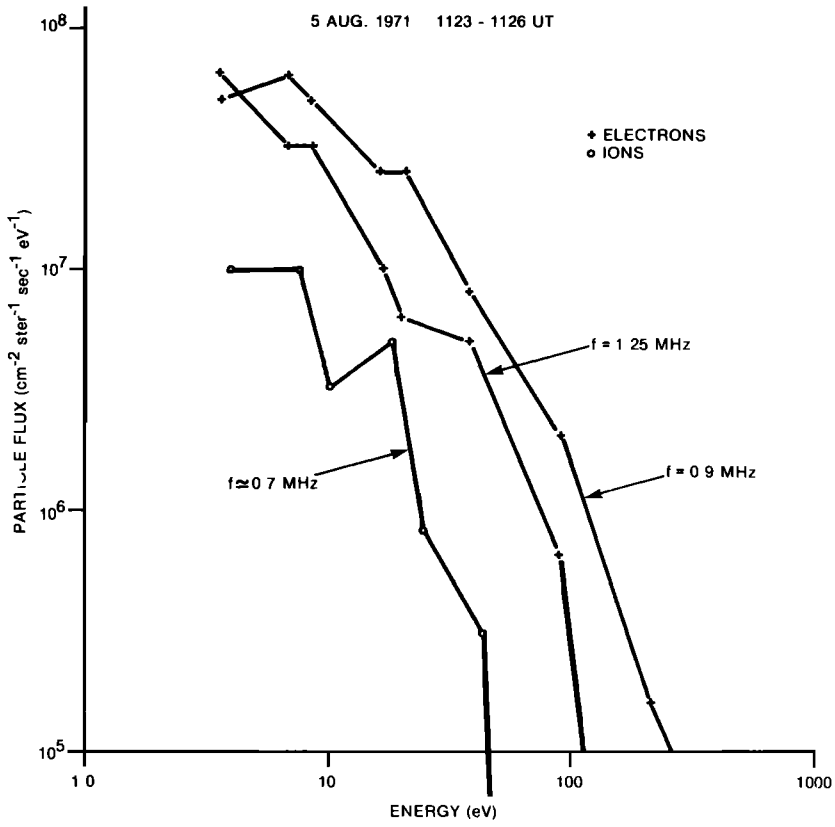

Fig. 15. SAP electron and ion energy spectra corresponding to data in Figure 6.

suggesting that spacecraft body protruberances cause the SPS ion aperture to be shadowed.

SAP Energy Spectra

Detailed spectra have been examined in some of the data sets for Figures 4–10. Figure 15 illustrates typical flux-versus-energy spectra taken from the same pass data as Figure 6. The electron spectra have been plotted for the two peaks in Figure 6: one spectrum corresponds to a sounder frequency just below f_{pe}, at 0.9 MHz. The other electron spectrum corresponds to the peak in Figure 6 at 1.25 MHz midway between f_{UH} and $2f_{ce}$. The ion spectrum corresponds to the peak at f_{ce}. Ion and electron spectra exhibit shapes similar to these at most frequencies of excitation.

The electron flux varies as (energy)$^{-2.0}$ above 10 eV. The ions typically have a rather sharp cutoff near their upper limit of about 100 eV. The flux densities of SAP electrons normally attain values such as shown in Figure 15. Ion peak fluxes are normally within 1 order of magnitude of the peak electron flux at energies of about 50 eV and are approximately equal below 10 eV.

SAP IN RELATION TO POTENTIAL OF THE SPACECRAFT BODY

General

The purpose of this section is to review a conventional picture of dc charging of an active spacecraft and to relate some of the SAP observations to that picture.

In a first attempt to understand SAP, trajectories of electrons accelerated by the rf near field of a dipole antenna were calculated. The equation of motion of a particle of mass m, charge q, and velocity $\mathbf{v}$, under the influence of the nonrelativistic Lorentz force is

$$m d\mathbf{v}/dt = q(\mathbf{E}_{rf} + \mathbf{v} \times (\mathbf{B}_{rf} + \mathbf{B}_0)). \quad (1)$$

Here, $\mathbf{E}_{rf}$ and $\mathbf{B}_{rf}$ describe the antenna near rf field and $\mathbf{B}_0$ describes the terrestrial magnetic field. Representative electron orbits were integrated using near-field expressions for a finite-length dipole in vacuum [*Jordan and Balmain*, 1968, p. 336].

The orbits traced indicated that, by itself, equation (1) is unrealistic for explaining SAP. Electrons starting with thermal speeds (kT = 0.1 eV) at points about 0.1 m away from the Y axis move to positions tens of meters distant from the dipole before the end of a 100 μs pulse. Speeds become quasi-relativistic near the gyrofrequency. Experimentally observed kinetic energies were achieved only after the orbits were clear of the spacecraft and therefore inaccessible to the SPS.

It thus appeared necessary to add other mechanisms, i.e., collective effects, to provide a satisfactory SAP model. There are two indications that collective effects are at work. One is that the distributions of electronic SAP flux versus exciting frequency peak in the vicinity of f_{pe} in Figures 4–10. The other indication is that ions are also accelerated, pointing to a dc electric field resulting from the rf.

It is proposed that the action of the rf pulse is to set up a rf sheath inside of which there is a deficiency of electrons. As explained by *Kasha* [1969] and references therein, a dc potential builds up on the spacecraft during an rf pulse. The potential provides an operating point that balances the time-integrated ion and electron currents to the spacecraft and antennas. For frequencies up to f_{pe}, the difference in elec-

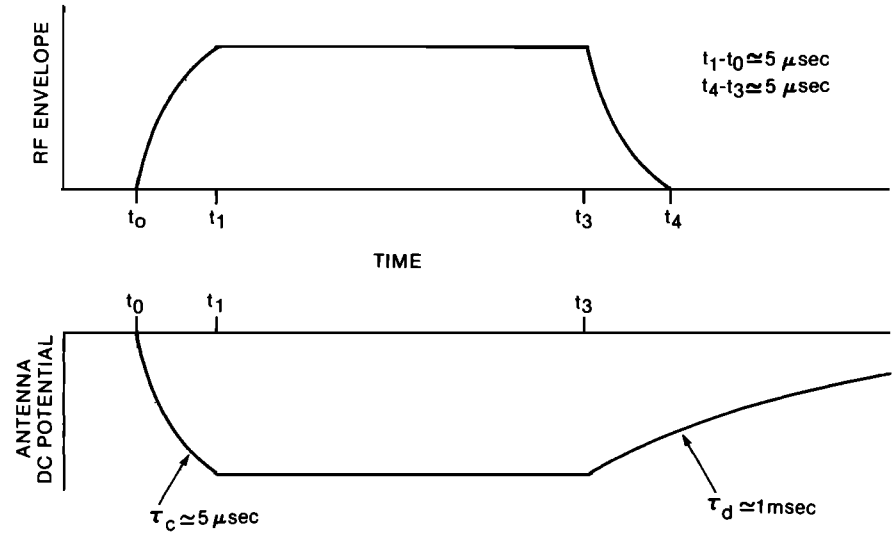

Fig. 16. Sounder rf pulse envelope and induced dc potential response.

tron and ion mobilities causes a rectification effect and results in a negative dc potential on the spacecraft [*Oya*, 1978]. As frequency increases above f_{pe}, the amplitude of electron motion decreases. Electron current collected by the antenna is reduced, resulting in positive antenna potentials at $f \gg f_{pe}$. Thus every pulse causes a charging, steady state, and a discharging sequence. The temporal relationship between the spacecraft dc potential and the applied rf potential is shown in Figure 16 for the case $f \lesssim f_{pe}$.

During the rf pulse, the Lorentz force and the induced dc sheath potential combine to force electrons into large-amplitude orbits centered near the sheath plasma interface [*Whale*, 1964; *Laframboise et al.*, 1975]. Individual particle orbits are described by equation (1) in which E_{rf} is augmented by a dc field term which tends to keep electrons near the sheath [*Whale*, 1964]. The sheath limit oscillates at the radio frequency. This steady state oscillation is maintained until the end of the pulse which has a falling edge lasting a few rf cycles (F. Daniels, private communication, 1982). Particle trajectories are then governed by the decaying negative dc potential on the antennas and spacecraft plus the Lorentz force due to $\mathbf{B}_0$ alone.

The interpretation is that SAP electrons are detected on ISIS II during the 100-μs rf pulse. As the instantaneous potential of the spacecraft body with respect to either monopole oscillates at the radio frequency about the dc potential, electrons of various energies, i.e., the observed electron spectrum, make their way to the SPS. The ions with the highest energy, corresponding to the steady dc body potential, also enter the SPS during the rf pulse. After the rf pulse, the dc decay effectively provides a downsweep in the detected ion energy. With reference to Figure 15, the sharp upper shoulder of the ion spectrum corresponds to rf pulse on, and the parts to the left are filled in progressively during the dc decay.

In the rectification domain, the time τ_c required to charge the antenna and spacecraft to the negative potential is estimated as $\tau_c = R_s C_A$, where R_s is the resistance associated with the electron-saturation current part of the antenna's *I-V* characteristic. C_A is the dipole capacitance. Following *Chen* [1965], the saturation current I is found by using

$$I = \tfrac{1}{4} n_e \bar{v} A q_e (1 + V/V_0)^{1/2}$$

and

$$R_s = V/I$$

in which

V voltage applied;
V_0 plasma potential;
n_e ambient number density;
$\bar{v}$ average electron thermal velocity;
A surface area of dipole;

and

q_e electronic charge.

The antenna capacitance C_A is estimated with the *Balmain* [1964] vacuum-limit expression

$$C_A = \pi E_0 L/(\ln [L/R] - 1)$$

in which L and R are, respectively, the dipole half-length and radius. Observed SAP ion energies are taken as an indication of the final potential V, to which the spacecraft is charged. Substituting the upper limit of $V = 250$, V_0 and $\bar{v}$ corresponding to a plasma temperature of 0.1 eV, $n_e = 10^4$ cm^{-3}, $L = 36.6$ m, and $R = 0.65$ cm, yields $\tau_c = 0.94$ μs. Thus the dc potential rises as fast as the rf pulse (~5 μs).

After the end of the applied rf pulse, the antenna-spacecraft system is discharged by the ion current drawn by the negative potential. The ion ram current

$$I = n_e v_s q_i L W_s \sin (\mathbf{L}, \mathbf{v}_s)$$

discharges the capacitance at a constant rate which we estimate by using C_A. That is, $I = C_A \Delta V/\Delta t$. In these expressions $\mathbf{v}_s$ = spacecraft velocity, $(\mathbf{L}, \mathbf{v}_s)$ is the angle between $\mathbf{v}_s$ and dipole direction vector $\mathbf{L}$, and W_s is the effective width of the antenna with sheath. By using sin $(\mathbf{L}, \mathbf{v}_s) = 1$, $W_s = 2R$ (a lower limit), and $v_s = 7100$ m/s, we obtain Δt (ms) = 0.009 V (volts).

In this computation, the effective width W_s is undoubtedly underestimated. A more realistic value is a few to several times $2R$, (J. G. Laframboise, private communication, 1982), in which case Δt is a few to several times too large. Thus it requires about 1 msec to discharge 250 V.

In the steady state part of the pulse, t_1 to t_3 in Figure 16,

the instantaneous voltage on either dipole arm periodically goes slightly positive. At this point in the cycle, it collects electron current which balances the modified ion ram current collected on the negative swing. This is the point in the cycle, therefore, at which the potential of SPS is presumed to rise to near zero and permit the low-energy SAP electrons to enter the SPS.

SAP electron peak energies (several hundred electron-volts) are typically higher than peak ion energies (100–200 eV). This is consistent with the picture in which the ions' energy indicates the dc antenna potential. Electrons may be pumped up to energies approaching 1 keV because they can follow the rf voltage swings of a few hundred volts about the dc potential. The directional properties of SAP in FIGURES 11–14 generally support this picture incorporating complicated electron motion and nearly linear motion to the SPS. That is, only electrons near $\theta = 90°$ are detected, whereas ions are isotropic except for the (presumed) antiram direction.

In general, the terrestrial magnetic field acts to skew the motion. Except for specialized cases such as antenna parallel to $\mathbf{B}_0$, stable orbits will not exist. Nevertheless, the effect of the sheath dc field is to counteract the rf forces and make it possible for some particles to stay close to the spacecraft while being energized and for some of them to be collected by the SPS. On the basis of the vacuum dipole theory, $\mathbf{B}_{rf}$ at a distance <1 m from the ISIS dipole with an antenna current of 1 A indicates that $\mathbf{v} \times \mathbf{B}_{rf}$ may be of the order of E_{rf} (~100 V/m) for energies >100 eV. Hence the rf Lorentz term must be retained for a general treatment of SAP at energies greater than 100 eV.

A quantitative analysis of electron motion is not attempted here. Because SAP electron fluxes collected depend on the details of the rf field-induced motion, an estimate of expected theoretical SAP flux levels is an extensive calculation. Ion flux, being influenced only by the dc potential and having more nearly linear motion to first order, can be more simply estimated. This is done in the following section.

Muldrew [1972] suggested that floating resonant spikes on topside sounder ionograms can be used to deduce a sheath collapse time. These are typically about 1 ms. This collapse time is assumed to be the same as the 1 ms discharge time estimated here. The sheath collapse observation thus provides independent support for the picture.

In an isotropic plasma, *Whale* [1964] predicts a resonance at $f = f_{pe}/2^{1/2}$. He shows that the nonlinear equation for an electron oscillating in an rf sheath predicts a natural oscillation of the sheath radius at this frequency. The published SAP data most relevant to the Whale approximation, i.e., with largest f_{pe}/f_{ce}, are those of *Gal'perin et al.* [1981, Figures 1, 2] and our Figure 4. It is interesting to note that the main SAP peak is displaced below f_{pe} by about the factor $2^{1/2}$.

In the search for an explanation of the frequency dependence of SAP, the evidence from topside sounders regarding ES wave resonances should also be considered. There is considerable evidence that anisotropic plasma heating is caused by ES wave absorption [*Oya*, 1971; *Oya and Benson*, 1972; *Kiwamoto and Benson*, 1979; *Benson*, 1982]. Because this heating takes place in the course of plane wave propagation, the heated volume must extend the order of 100 m from the spacecraft. By contrast, SAP electrons are gathered from distances that may be as large as 10–20 m, but more likely are of the order of their gyroradius, i.e., 1 m.

Also, note that collective oscillations of a hot plasma in a cylindrical geometry will produce resonances characteristic of that geometry. *Whale*'s [1964] resonance at $f_{pe}2^{1/2}$ is an example. In view of all of the above, it appears difficult at this stage to predict cylindrical sheath resonances on the basis of eigenfrequencies for true wave heating already reported (*Benson* [1982] and references therein).

Ion Data

The SAP distributions as a function of frequency, Figures 4–10, indicate that ionic SAP is observed below and up to about the greater of f_{pe} and f_{ce}, but not above. That is, the production of the hypothesized dc potential appears limited to the resonant frequency domains of the plasma. There are oblique cone resonances in the range 0.1 MHz to min (f_{pe}, f_{ce}) and max (f_{pe}, f_{ce}) to f_{UH}, and electrostatic resonances near f_{pe}, nf_{ce}, and f_{UH}. Resonant electron motion and the associated large orbits thus seem to be necessary for the large negative dc potentials.

The dependence of SAP flux on frequency in Figures 4–10 implies that the characteristic electron frequency region is the borderline between negative dc spacecraft potential (below f_{pe} and f_{ce}) and positive potential (above f_{pe} and f_{ce}). The charge and discharge times estimated above assumed a negative potential due to the predominance of the rectification effects [*Kasha*, 1969; *Shkarofsky*, 1972]. However for $f > f_{pe}$, electron motion in response to the rf field is more restricted. Electrons do not flow to and from the antenna but rather execute smaller orbits about an average sheath limit [*Whale*, 1964; *Laframboise et al.*, 1975]. With electron current thus reduced ion ram current tends to predominate. The result is that the average potential is now a small positive value and SAP ion energization is cut off.

The terrestrial magnetic field undoubtedly complicates the models of *Whale* [1964] or *Laframboise et al.* [1975]. SAP electrons are clearly present and SAP ions are absent at $f = 2f_{ce}$ in Figures 7–10. Apparently the $2f_{ce}$-resonant electron current to the spacecraft is not large enough to affect the body potential significantly.

In the rectification case, SAP ion fluxes are expected to show a slight dependence on the 'ram' angle, β. The collected ions, assumed to be protons, have kinetic energies of several tens of electron volts, compared with the ram energy of 0.26 eV. The extent to which the kinetic energy exceeds the ram energy determines how close to complete symmetry in angle β are the ion trajectories entering the SPS.

Figures 13 and 14 illustrate relatively flat pitch angle distributions for $60° < \beta < 120°$. Disregarding a sharp notch seen in other data at $\beta < 60°$ or $\beta > 120°$, the flux can be taken as isotropic in β at the spacecraft body surface. At the same time, it must be remembered that the trajectories of ions traced backwards in time are all eventually parallel to the spacecraft velocity. That is, at a great enough distance from the spacecraft, of the order of 1 m, the spacecraft collects its current in the ram direction (J. Laframboise, private communication, 1982).

Theoretically, the ion current I swept up by a spherical satellite body of effective radius R_e is $I = n_e v_s \pi R_e^2$. Assume that ions are collected over 2π st at each surface element of the spacecraft body and over all the actual body area, $4\pi R_B^2$, where R_B is the body radius. If G is the SPS geometrical factor for ions, then the current into the SPS is estimated as

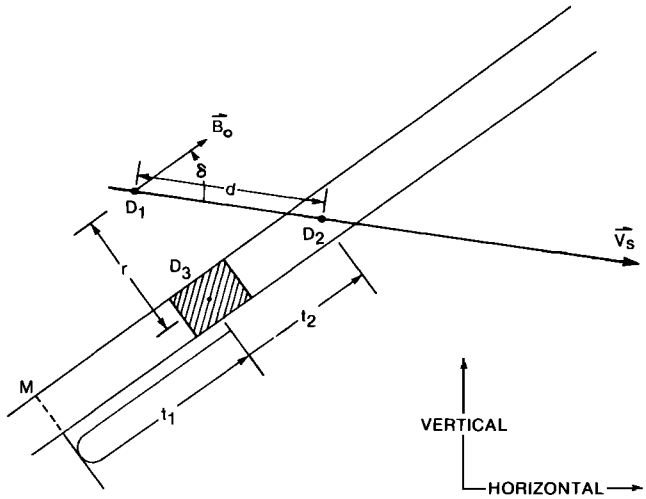

Fig. 17. Geometry of SAP electrons mirroring near ISIS I for the plane containing the spacecraft velocity $\mathbf{v}_s$ and the local magnetic field $\mathbf{B}_0$. The sounder dipole is generally at some oblique angle with respect to the $\mathbf{v}_s$-$\mathbf{B}_0$ plane.

$IG/2\pi 4\pi R_B^2$. The time during which the negative potential is on the spacecraft is taken as $\tau_d \simeq 1$ ms (Figure 16). Therefore the total count into the SPS per rf pulse = $IG\tau_d/2\pi 4\pi R_B^2$. Using again $n_e = 10^{10}$ m^{-3}, $v_s = 7100$ m/s, one finds that total count = $0.28 \times 10^6\, G\, R_e^2/R_B^2$.

Observationally, a differential flux of 10^7 cm^{-2} st^{-1} s^{-1} eV^{-1} corresponds to a total count of $10^7 \times G \times (1/90) \times 50 = 0.055 \times 10^6\, G$ when using a typical 50 eV energy range for the ions.

The two counts are equal if $R_e = 2.2\, R_B$. The ISIS spacecraft has $R_B \simeq 0.6$ m, and it is reasonable in the light of other evidence [*James*, 1980] that the rf sheath has an effective radius of 1.3 m.

The proposed model is based on zero net current to the spacecraft integrated over the sounder pulse repetition period (22.2 ms on ISIS II). The electron and ion differential fluxes are most intense at the lowest measurable energy, 5 eV. At this energy, ions and electrons are observed by the SPS over most of the 0° to 180° pitch angle range. Therefore, they can be collected over most of the 2π st solid angle subtended by any surface element. Hence, the equality of peak differential fluxes demonstrates the current balance.

ISIS I Evidence

From a data set of roughly 500 ISIS I spectrograms, SAP electrons have been identified on five equatorial perigee passes. ISIS I has a sounder PRF of 30^{-1}s and the pulse is timed to be on during the SPS readout time. As shown in Figure 2, a delay time, τ_r (4.69 ms), between the rf pulse transmission and the beginning of the next SPS sample period is the minimum delay of SAP in order that it be observed on ISIS I. *Gal'perin et al.* [1981] deduced that SAP may persist up to 3 ms after the sounder pulse.

The geometry required in order that ISIS detect SAP is shown in Figure 17. At time t_0, ISIS I is at point D_1 and has just finished an rf pulse. This results in a energized plasma extending out to a cross-field distance of at least r. At $\tau_r + t_0$ the spacecraft has moved d metres to point D_2. There, it detects 100 eV particles with pitch angle α close to 90° that have orbited along a flux tube with the radius equal to the gyroradius appropriate to that energy.

Twenty separate instances of SAP have been found in the five ISIS I passes. In this data set, the angle δ varied between 4° and 28°, and r, correspondingly, varied between 3 and 18 m.

The electrons are detected at point D_2 with the SPS viewing axis at = 90° ± 15°. However, the finite width of the SPS viewing aperture is 25°, which means that this uncertainty must be added to the stated value. The pitch angle resolution is not adequate for making deductions about the source of the energized electrons.

An equatorial pass of ISIS I on April 26, 1969, at 0922 UT has been analyzed by computing the trajectory of a single unperturbed electron in a centred dipole field. In one particular case SAP electrons were observed at energies up to 200 eV at a dip latitude of 14.3° and a height of 712 km. Trapped particle motion was analyzed to find the bounce trajectory that corresponds to the observed total delays $\geq \tau_r$. The spacecraft spin axis, $+Z$ in Figure 1, was within 20° of $-\mathbf{B}_0$ and hence the dipole remained close to perpendicular to $\mathbf{B}_0$. It was therefore hypothesized that electrons were energized at positions located cross-field from the satellite body. In Figure 17, the electrons detected at D_2 were assumed to be in the cross-hatched region D_3 at the end of the rf pulse. The rf pumping leads to one of two possibilities: the electron moves from D_3 to D_2 directly, or it orbits from D_3 to its near mirror point M, then goes back through D_3 to D_2. Expressions used to evaluate the two transit times for arbitrary start pitch angle and energy are given in the appendix.

For 100-eV electrons in the case in point, a total transit time of at least 4.69 ms required an orbital path through D_3–M–D_3–D_2. In order that the transit time, $t_1 + t_2$, equal 4.7 ms, the starting pitch angle α_0 had to be 89.96°, the distance r, 17.9 m, and α at point D_2, 89.82°. Progressively longer delays corresponded to smaller values of α and larger r's.

Similar pitch angles were found for the other ISIS I cases of equatorial SAP electrons arriving at least 4.69 ms after the rf pulse. The ISIS I spacecraft body structure is such that the SPS aperture is magnetically shadowed for 100-eV electrons near 90°. Since the SPS entrance is 10 cm from the $+Z$ end of the spacecraft, and since this was the end facing the supposed direction from which mirroring particles approached the spacecraft, the situation was most favorable for electrons to enter the SPS. A calculation using approximate spacecraft dimensions showed that particles with $\alpha < 89.52°$ could enter the SPS.

For the case in point the computations showed that electrons passing through D_3–M–D_3 and arriving at point D_2 on Figure 17 with $\alpha < 89.52°$ had $t_1 + t_2 > 17.6$ ms and $r > 67$ m. Electrons could also go directly from D_3 to D_2 in 0.1 ms. Hence if magnetic shadowing was correctly estimated, it imposed severe restrictions on the observation of SAP. It also implied that a much greater volume of SAP is energized around the spacecraft than implied by a delay of 4.69 ms.

When all the SAP data from the April 26, 1969, pass were considered, it was concluded that magnetic shadowing must have been circumvented. At 0926 UT, SAP was detected with $\delta = 6°$, which would have required an even longer delay, $t_1 + t_2$. A total delay of either 0.1 or 17.6 msec would place all SAP created by the ISIS I sounder pulses in SPS 'READ' intervals. Throughout the pass, delay times required for the D_3–M–D_3–D_2 path were of the order of 20 ms. Since the SPS cycle period = 1/60 s, this would produce

'spill-over' on the ISIS I spectrograms. No obvious exceptions to the one-on, one-off signature of SAP were found on ISIS I, whence it was deduced that delay times $t_1 + t_2$ were considerably smaller than required by $\alpha < 89.52°$.

The uncertainty is spacecraft dimensions is not sufficient to bridge the α gap between the critical shadowing condition, $\alpha = 89.52°$, and the final α, 89.82°, corresponding to the minimum delay, 4.69 ms. For these reasons, it was concluded that some sort of perturbing electric field acted to bridge the α gap.

Slowly varying electric fields are one possibility. Natural perpendicular electric fields may be able to adjust the trajectories. More likely, the spacecraft dc potential could favourably deflect incoming electrons. The restriction of ISIS I SAP observations to equatorial perigee passes indicates that special ionospheric conditions are necessary for the creation of the perturbation, whatever it may be.

Another possibility is that the SAP beam loses its coherence on the time scale of 10 ms. That is, Landau damping scatters SAP electrons into the SPS acceptance beam. This would be similar to the damping experienced by propagating waves, to which *Gal'perin et al.* [1981] and *Benson* [1982] refer. The existence of nonlinearly produced signals in sounder ionograms is attributed to instabilities that follow the production of anisotropic temperatures arising from Landau damping of electron cyclotron waves.

On the basis of the ISIS I data, it is difficult to distinguish between dc fields and collective effects as being responsible for long-delay SAP. If the original rf-impressed signal phase were retained for milliseconds, a radio receiver turned to f_{ce} would detect a signal from the coherently bunched particles. However, its magnitude would be much smaller than the field of passing waves and therefore masked by them. Also, the signal level would be below the threshold of the ISIS sounder receiver.

In the April 26, 1969, example, SAP was detected every second time the sounder swept through f_{ce}. This appears due to the alternately favorable and unfavorable proximity of the antenna to the cross-hatched area in Figure 17. In this pass, 2 × sweep period = 2.5 × spin period. A computation of the instantaneous dipole positions showed that SAP was received when the minimum separation of the dipole and the flux tube sampled by the SPS at D_2 was less than roughly 11 m, assuming detection at $t_1 + t_2 = 4.69$ ms.

The transit analysis indicates why long delay ($\tau_r = 4.7$ ms) SAP is not observed on ISIS II: the body structure is different and shadows the SPS for a wider range of pitch angles. On ISIS II the distance to the $+Z$ extremity from the SPS is about 33 cm, corresponding to a minimal forbidden zone of 86.8° to 90° for $E = 100$ eV and $f_{ce} = 1$ MHz. Hence the 'α gap' for long-delay SAP is considerably greater on ISIS II (a few degrees) than on ISIS I (a fraction of a degree).

When the SPS data were compared with the corresponding sounder ionograms on all five ISIS I passes with SAP, it was found that the SAP spikes were each associated with some harmonic of f_{ce}. In the 26 April 69 pass, time-resolved measurements of four SAP spikes were recorded. These spikes were centred at the times when the sounder frequency $= f_{ce}$, to good accuracy. In succession, the SAP spikes widened from 1 to 2 s. This progression is interpreted as due to an increase of the intensity of the rf field in the flux tube D_3–D_2 shown in Figure 17 due, in turn, to a decreasing separation r. At high intensities, side bands of the pulse are able to cyclotron-pump particles even when the carrier frequency, f_0, is displaced by a few tens of kHz from f_{ce}. At the larger r values, the field is strong enough to excite SAP only when $f_0 = f_{ce} \pm 10$ kHz.

Concluding Remarks

The principal results of this work on sounder-accelerated particles are as follows:

1. SAP electrons and ions have typical energy ranges up to 300–500 eV and 100–200 eV, respectively. Electrons are detected in a restricted pitch angle range about 90° that depends on energy. Ions have little pitch angle dependence.
2. A model for the rf-induced spacecraft potential has been described in which electrons of all energies and ions of highest energies are collected during the 100 μs rf field. Lower energy ions are collected during a 1-msec discharge period following the pulse.
3. SAP ion and electron fluxes are most intense near but not at the electron plasma and gyrofrequencies. This suggests that the intrinsic antenna impedence or characteristic resonances of the sheath complicate the energization scheme.
4. SAP ion fluxes are cut off for sounder frequencies near f_{pe}. As anticipated by published theory, the plasma frequency is roughly the crossover frequency between rectification control (below f_{pe}) to the situation above f_{pe} in which the finite induced electron motion limits the dc spacecraft potential.
5. SAP electrons observed milliseconds after the sounder pulse require sounder frequencies at one of the gyroharmonics and pitch angles very close to 90°. However, in order to enter the SPS, the electron trajectories require some perturbation.

The creation of substantial charged particle fluxes by HF transmitters in the ionosphere has important implications for active experiments in space physics. Because SAP energies and flux intensities are comparable to natural particle fluxes, such as precipitation at high latitudes, SAP probably triggers ostensible wave phenomena near the sounders [*Oya*, 1978; *Benson*, 1982]. The analysis of any of the variety of (nonlinear) waves heretofore observed should take into account the participation of SAP. For example, there is evidence (D. B. Muldrew, private communication, 1982) that SAP ions are responsible for a periodic signal excited at whistler mode frequencies called 'candles.'

The SAP observations provide information about the rf sheath around, and the dc potential of, an active antenna. SAP data may thus be used to improve theories about the sheath contribution to driving-point load of an antenna. They may also be used to infer the contribution to waves truly radiated by an antenna, waves that arise from the SAP currents themselves. The arguments presented here regarding spacecraft dc body potential lead to the idea that rf might be used to control, or at least to study, spacecraft potentials and related parameters. By judicious choice of the transmitting frequency, typically close to local f_{pe} or f_{ce}, a large negative potential could be induced on a spacecraft.

On a broader outlook, the use of tunable HF transmitters as particle sounders can be foreseen. The SAP flux levels published here are capable of being used as tracers of field lines, using conventional spectrometers. On some scale that will be limited by electron beam dynamics, SAP fluxes could be used for particle bounce experiments to map field lines,

and thus to measure associated large-scale effects like convection. Energization with an rf pulse leads to SAP fluxes that are phase-bunched. Therefore SAP injection has an inherent advantage over other techniques for energetic particle tracing in space.

APPENDIX

The expressions for charged-particle mirroring in a dipole magnetic field given by *Roederer* [1970] have been modified to represent bounce motion to and from a general geomagnetic latitude λ as follows: a particle starts at a latitude λ_0 with pitch angle α_0, mirrors at latitude λ_m, and returns to λ_0 in total time τ_b. The time τ_b is the integral over field-aligned distance s of the reciprocal parallel velocity $v_{\|}(s)$:

$$\tau_b = 2 \int_{\lambda_0}^{\lambda_m} \frac{ds}{v_{\|}(s)} \tag{A1}$$

Roederer's equation (2.2) is used in the form $v_{\|}(s) = v \cos \alpha = v\,[1 - \sin^2 \alpha_0 (B_0(\lambda)/B_0(\lambda_0)]^{1/2}$. His equation (2.51) is applied as written. The ratio

$$\frac{B_0(\lambda)}{B_0(\lambda_0)} = \frac{(4 - 3\cos^2\lambda)^{1/2}\cos^6\lambda_0}{(4 - 3\cos^2\lambda_0)^{1/2}\cos^6\lambda} \tag{A2}$$

then permits us to write the generalization of Roederer's (2.61a) as:

$$\tau_b = \frac{2r_0}{v} \int_{\lambda_0}^{\lambda} \cos\lambda \sqrt{4 - 3\cos^2\lambda}\, d\lambda/\text{denom} \tag{A3}$$

in which the denominator is

$$\text{denom} = \left[1 - \sin^2\alpha_0 \frac{(4 - 3\cos^2\lambda)^{1/2}\cos^6\lambda_0}{(4 - 3\cos^2\lambda_0)^{1/2}\cos^6\lambda}\right]^{1/2} \tag{A4}$$

Bounce time τ_b has been computed numerically, using λ_m found with

$$\sin^2\alpha_0 = \frac{(4 - 3\cos^2\lambda_0)^{1/2}\cos^6\lambda_m}{(4 - 3\cos^2\lambda_m)^{1/2}\cos^6\lambda_0} \tag{A5}$$

With reference to Figure 17, expression (A3) gives the time t_1 directly and the time t_2 when λ_m is replaced by the final latitude of D_2 and the 2 is replaced by a 1.

Acknowledgments. The author is much indebted to D. M. Klumpar and W. J. Heikkila of the University of Texas at Dallas and to J. D. Winningham of the Southwest Research Institute for their kind help in providing the ISIS soft particle spectrometer data.

The editor thanks R. F. Benson and A. C. Calder for their assistance in evaluating this paper.

REFERENCES

Balmain, K. G., The impedance of a short dipole antenna in a magnetoplasma, *IEEE Trans. Antennas Propag., AP 12*(5), 605–617, 1964.

Balmain, K. G., The properties of antennas in plasmas, *Ann. Telecommun., 35*(3–4), 273–283, 1979.

Benson, R. F., Stimulated plasma instability and nonlinear phenomena in the ionosphere, *Radio Sci., 17*(6), 1637–1659, 1982.

Chen, F. F., Electric probes, in *Plasma Diagnostic Techniques*, edited by R. H. Huddlestone and S. L. Leonard, pp. 113–200, Academic, New York, 1965.

Franklin, C. A., and M. A. Maclean, The design of swept-frequency topside sounders, *Proc. IEEE, 57*(6), 897–929, 1969.

Gal'perin, Yu. I., R. Z. Sagdeev, F. K. Shuiskaya, Yu. V. Lisakov, V. V. Migulin, Yu. V. Kushnerevskii, M. D. Fligel', and G. V. Vasil'ev, Detection of electron acceleration in the ionospheric plasma under the influence of high-power radio radiation near the local plasma frequency aboard the space vehicle Interkosmos 19, *Cosmic Res., 19*(1), 22–29, 1981.

Getmantsev, C. G., and N. G. Denisov, Concerning an effect during measurement of electron concentration in the ionosphere by the antenna probe method, *Geomagn. Aeron., 2*(4), 575–577, 1962.

Hagg, E. L., E. J. Hewens, and G. L. Nelms, The interpretation of topside sounder ionograms, *Proc. IEEE, 57*(6), 949–960, 1969.

Heikkila, W. J., J. B. Smith, J. Tarstrup, and J. D. Winningham, The soft particle spectrometer in the ISIS-I satellite, *Rev. Sci. Instrum., 41*(10), 1393–1402, 1970.

James, H. G., Tests of impedance theories for a transmitting dipole in an ionospheric plasma, *IEEE Trans. Antennas Propag., AP 28*(5), 623–630, 1980.

Johnston, T. W., Time-averaged effects on charged particles in A-C fields, *RCA Rev., 21*(4), 570–610, 1960.

Jordan, E. C., and K. G. Balmain, *Electromagnetic Waves and Radiating Systems*, Prentice-Hall, Englewood Cliffs, N. J., 1968.

Kasha, M. A., *The Ionosphere and its Interaction With Satellites*, Gordon and Breach, New York, 1969.

Kiwamoto, Y., and R. F. Benson, Nonlinear Landau damping in the ionosphere, *J. Geophys. Res., 84*(A8), 4165–4174, 1979.

Laframboise, J. G., J. Rubenstein, and F. H. Palmer, Theory of topside sounder transmissions effects on antenna quasistatic sheath impedance, *Radio Sci., 10*(8, 9), 773–784, 1975.

Lockwood, G. E. K., Side band and harmonic radiation from topside sounders, *J. Geophys. Res., 78*(13), 2244–2250, 1973.

Muldrew, D. B., Electron resonances observed with topside sounders, *Radio Sci., 7*(8, 9), 779–789, 1972.

Oya, H., Verification of theory on weak turbulence relating to the sequence of diffuse plasma resonances in space, *Phys. Fluids, 14*(11), 2487–2499, 1971.

Oya, H., Generation mechanism of proton cyclotron echoes due to pulsed radio frequency waves in space plasma, *J. Geophys. Res., 83*(A5), 1991–2008, 1978.

Oya, H., and R. F. Benson, A new method for in situ electron temperature determinations from plasma wave phenomena, *J. Geophys. Res., 77*(22), 4272–4276, 1972.

Roederer, J. G., *Dynamics of Geomagnetically Trapped Radiation*, vol. 2, *Physics and Chemistry in Space*, Springer-Verlag, New York, 1970.

Shkarofsky, I. P., Nonlinear sheath admittance, currents and charges associated with high peak voltage drive on a VLF/ELF dipole antenna moving in the ionosphere, *Radio Sci., 7*(4), 503–523, 1972.

Whale, H. A., Ion sheath effects near antennas radiating within the ionosphere, *J. Geophys. Res., 69*(3), 447–455, 1964.

(Received September 22, 1982;
revised January 14, 1983;
accepted February 16, 1983.)